Biochem. Cell. Arch. Vol. 18, No. 1, pp. 245-258, 2018 | www.connectjournals.com/bca | *ISSN 0972-5075*

OPTIMIZING PET-CT IMAGE RECONSTRUCTION PARAMETERS FOR DIAGNOSTIC IMAGING USING NON-TOF ALGORITHMS

Zainab Shamkhi Jaber[1]*, Babak Fallahi[2], Parham Geramifar[2] and Marzieh Ebrahimi[2]

[1]Department of Radiology and Radiotherapy, Allied School, Tehran University of Medical Sciences, Tehran, Iran.
[2]Research Center for Nuclear Medicine, Shariati Hospital, Tehran University of Medical Sciences, Tehran, Iran.

(Accepted 27 February 2018)

ABSTRACT : ^{18}F-fluorodeoxyglucose positron-emission tomography/computed tomography (FDG-PET/CT) reconstruction algorithms can have substantial influence on quantitative accuracy especially for diagnostic oncology. The goal of this study was to optimize PET-CT image reconstruction parameters for diagnostic image using non-TOF algorithms by evaluating the effect of number of iterations and subsets(sub-iterations) in the reconstruction process with and without resolution recovery in four different tumour to background ratios (TBRs). We analyzed radial activity concentration profiles for different lesion sizes in PET/CT images and calculate recovery coefficient (RC), contrast to noise ratio (CNR), noise and coefficient of variation(COV) besides activity concentration distribution (Bq/cc) and standardized uptake value (SUV) measurement.

Measurements were performed on the Siemens Biograph 6 true points PET/CT scanner (SIEMENS, Erlangen, Germany), using a cylindrical phantom filled with five hot syringes with various diameters (0.5, 0.9, 1.3, 1.6, 2.2cm). The acquisition was done four times with different TBRs (8:1, 6:1, 4:1, 2:1). The images were attenuation corrected using low dose CT images (110kV, 31mA). The reconstruction parameters were iterative, iterative 3D and TrueX (resolution recovery in SIEMENS) reconstruction algorithms with 1-8 iterations and 4,8,14, and 21 subsets in 128x128 matrix size which results in totally 1380 different configurations. It should be noted in all reconstructions, a post smoothing filter with 5mm Full width Half Maximum (FWHM) was used.

CNR values were higher than five threshold value, for all the syringe sizes and TBRs except for the syringe size 0.5 in TBR 6:1, 0.9 in TBR4:1, and 2.2 in TBR 2:1. RC Values reported for iterative 2D and iterative 3D has large bias in comparison to TrueX reconstruction algorithm which makes worse in lower number of sub-iterations.

Reconstruction parameters can significantly affect SUV and quantification measurements. The optimized reconstruction TrueX algorithm was proposed for PET/CT diagnostic imaging.

Key words : PET/CT, ^{18}F- FDG, Reconstruction Algorithms, CNR.

INTRODUCTION

The development of nuclear medicine has resulted in several effective routine methods in diagnosis and therapy. There is an ongoing discussion about the future of the activity based on the fast development of ultrasound, CT and MR. In such discussions, it is often forgotten that nuclear medicine is also a dynamic diagnostic tool under continuous progress. Nuclear medicine has grown from quite simple *in vitro* tests to very advanced methods to image organ function. This is the result of the development of radiopharmaceuticals and instrumentation (Carlson, 1995).

In these test, small amounts of radiopharmaceuticals are introduced into the body by injection, swallowing, or inhalation. They are substances that are attracted to specific organs, bones, or tissues. The amount of radiopharmaceutical used is carefully selected to provide the least amount of radiation exposure to the patient but ensure an accurate test. A special camera (PET, SPECT or gamma camera) is then used to take pictures of your body. The camera detects the radiopharmaceutical in the organ, bone or tissue and forms images that provide data and information about the area in question. Nuclear medicine differs from an x-ray, ultrasound or other diagnostic test because it determines the presence of disease based on biological changes rather than changes in anatomy (Society of Nuclear Medicine).

An integrated PET/CT system opens the door for integrating biologic volumes from PET with the anatomic volumes from CT into the process of radiation treatment planning, which traditionally has relied on anatomic information alone (Ruth *et al*).

The aim of PET/CT implementation is detecting and localizing malignant lesion to assess cancer staging with providing functional and anatomical information to assess

**Corresponding author*

metabolism, metabolic size, and proliferation—critical parameters for determining the outcome of radiation therapy (Teo *et al*, 2007).

With PET/CT, the radiation dose to the patient is the combination of the radiation dose from the PET radiopharmaceutical and the radiation dose from the CT portion of the study. Radiation dose in diagnostic CT has attracted considerable attention in recent years, in particular for pediatric examinations. It can be very misleading to state a ''representative'' dose for a CT scan because of the wide diversity of applications, protocols, and CT systems (Delbeke *et al*, 2006).

The most popular PET tracer is 2-[^{18}F] fluoro-2-deoxy-D-glucose ([^{18}F] FDG), which allows visualization of glucose metabolism. Therefore, [^{18}F] FDG is widely used for the diagnosis of cancer and monitoring of cancerous lesions that often show increased glucose metabolism (Fig. 6).

^{18}F-FDG PET and CT are proven diagnostic procedures. Although, techniques for registration and fusion of images obtained from separate PET and CT scanners have been available for several years, the readily apparent and documented advantages of having PET and CT in a single device have resulted in the rapid dissemination of this technology in the United States. This Procedure Guideline pertains only to combined PET/CT devices (Delbeke *et al*, 2006).

Each PET-CT scan itself generates a considerable volume of raw image data which must be reconstructed, and the reconstructed images distributed and archived without impeding overall workflow. PET-CT facility design and layout, the procedures for sequencing patients through each phase of the exam, and adequate staffing are important considerations for an efficient and high-quality service (Faasse and Shreve, 2008).

PET acquisition parameters, such as acquisition mode, scan duration per bed position, and amount of bed overlap in subsequent bed positions, in combination with patient weight and 18F-FDG dose, affect PET image quality. Poorer image quality (increased noise levels) may result in an upward bias of SUV measurements. To optimize image quality, recommendations are generally given for uptake period, scan duration, and 18F-FDG dose. The dose can be selected from a range of generally used doses (Tong *et al*, 2010).

Through different algorithms, PET data can be reconstructed into the spatial distribution of a radiotracer. PET imaging provides noninvasive, quantitative information of biological processes and such functional information can be combined with anatomical information from CT scans. The integration of PET and CT on modern PET/CT scanners provides a synergy of the two imaging modalities, and can lead to improved disease diagnosis and treatment monitoring (Ng *et al*, 2013).

Modeling the statistical noise of PET data and the physical effects of the imaging model can lead to improved performance over the analytical methods. The improvement, however, comes at the expense of increased complexity of the reconstruction problem, making it impossible to obtain a direct analytic solution. Consequently, the reconstruction problem is solved iteratively, meaning the image estimate is progressively updated towards an improved solution. Initially, the computation cost hindered iterative reconstruction's clinical use, but advances in computation speed and the development of efficient algorithms have permitted widespread clinical use of iterative image reconstruction methods (Moscariello *et al*, 2011).

PET quantification based on standardized uptake values (SUV) is hampered by several factors, in particular by variability in PET acquisition settings and data analysis methods (Makris *et al*, 2013).

To measure SUV, a 2D or 3D region of interest (ROI) is positioned centrally within a target (*i.e.*, tumor) using an interactive workstation. The measured radioactivity within the ROI is normalized to the average radioactivity concentration in the body, which is approximated as the injected dose divided by patient body size. Common body size measurements are based on the patient's body weight, lean body mass, or body surface area, with body weight being the most frequently used (Adams *et al*, 2010).

Another important parameter is tumor to background ratio (TBR) a unique parameter that used only in studies of PET imaging, which was introduced in the literature in 2006 and has been widely used in publications thereafter. TBR varies as a function of how lesion activity are measured. The methods are variable in the published studies (Chen and Dilsizian, 2015).

MATERIALS AND METHODS

PET-CT acquisition setup

The current study was performed using a Siemens Biograph 6 True point PET-CT scanner, was used for acquiring and reconstructing the PET/CT images, equipped with resolution recovery (RR). The coincidence window is set to 4.5 ns and the patient port aperture is 70 cm. In all studies, low-dose CT scans are obtained prior to PET scans, used for attenuation and scatter corrections. Low-dose CT scans are obtained prior to PET scans, used for attenuation and scatter corrections. KV = 110 and mAs=31.

Phantom study

A Jaszczak phantom containing five hot syringes (internal diameters 0.5, 0.9, 1.3, 1.6 and 2.2cm) was filled with a uniform concentration of ^{18}F-FDG to achieve 8:1; 6:1; 4:1; 2:1 tumor -to-background ratio (TBR). TBR was selected so that a high tumor uptake in comparison to the background was realized. The volume of the phantom was 4 liters and it was initially filled with the activity concentration of 185, 185, 114, 185MBq mL^{-1} of ^{18}F-FDG. The whole phantom was centered in the FOV of the PET scanner and the images were acquired at a single-bed position. Detector events of PET/CT acquisition were collected for 5 minutes and the phantomswere imaged with one bed position for every phantom.

Uniform cylindrical phantoms are used routinely to normalize and calibrate scanners and to qualify scanners for quantitative imaging in clinical trials. However, phantom scans can also add value to a PET-CT quality control program in monitoring calibrations over time, identifying artifacts, and investigating problems (Medical Uses of Radioactive Materials).

PET/CT measurement

For the Siemens Biograph 6 PET/CT scanner, ^{18}F-FDG is used as a good tracer to detect subject uptake value of tumors.

For the acquisition time of this thesis (5 min) and the half-life of ^{18}F(109.771 min), it should be noted that the measured activity of ^{18}F-FDG is a result of electron energy depositions whereas PET/CT image is formed based on photons created through positron annihilations. As such, for the activity concentrations based on the PET/CT reconstructed images, both of true and imaging value of ^{18}F-FDGis also considered.

The initial activity concentrations (true values) in hot syringes were 0.3544, 0.2682, 0.1112, and 0.0914 MBq mL^{-1}for 8:1; 6:1; 4:1; 2:1 tumor-to-background ratio, and the results were compared to the activity concentrations measured from PET/CT images (image value).The true values of background and syringes were different for each of thesephantoms are shown in Table 1.

Image reconstruction

In this study, four OSEM reconstruction parameters were adopted: the number of iterations (Ni), the number of subsets per iteration (Ns), the smoothing filter, and the application of resolution recovery technique (HD). The attenuation and scatter corrected sinograms were applied using low-dose CT images. The applied post smoothing filters include all-pass, as well as Gaussian filter with full width at half maximum (FWHM) value of 5mm.

We consider a set of sub-iterations or $N_i \times N_s$ values as below :

A = {4, 8, 12, 16, 20, 21, 24, 28, 32, 40, 42, 48, 56, 63, 64, 70, 84, 98, 105, 112, 126, 147, 168}

To investigate the impact of increasing the iteration on the detectability and quantitative accuracy, one to eight iterations were considered.

For each activity concentration, the raw data are reconstructed based on the described variations, and the impacts of reconstruction parameters on the detectability performance and quantitative estimation were evaluated.

PET/CT images were reconstructed both with PSF modeling (TrueX Reconstruction) and without PSF modeling (2D and 3D iterative OSEM algorithms).

Data analysis

To evaluate the impact of reconstruction parameters on the detectability performance and quantitative accuracy, contrast to noise ratio (CNR), activity recovery coefficient, precision, and accuracy were calculated for various reconstruction parameters.

CNR and detectability

Since the small positron branching ratio of ^{18}F results in weak signals for this radionuclide compared to the common PET tracers, lesion detection with ^{18}F PET imaging has been the subject of some research.

It should be noted that higher lesion-to-background ratios correspond to enhanced image contrast. At the same time, statistical noise levels also play an important role in detection performance of lesions incorporating ^{18}F and they should be considered as well. Consequently, contrast-to-noise ratio (CNR) index based on the following formula is a more thorough metric to assess detectability performance using the Rose criterion. Based on the Rose criterion, an object is considered discernible when the calculated CNR values exceeds ~5 (Cherry and Me (2003).

$$CNR = \frac{C_{Lesion} - C_{Background}}{\sigma_{Background}} \quad (1)$$

Where, C_{Lesion} and $C_{Background}$ denote the lesion and the background signals respectively and $ó_{Background}$ is the variability in background intensity.

These background ROIs were selected, in such a way that they are at least three voxels a way from each other and at least four voxels a way from phantom boundaries. Hence, the correlations between ROIs were avoided and various statistically independent ROIs were implemented.

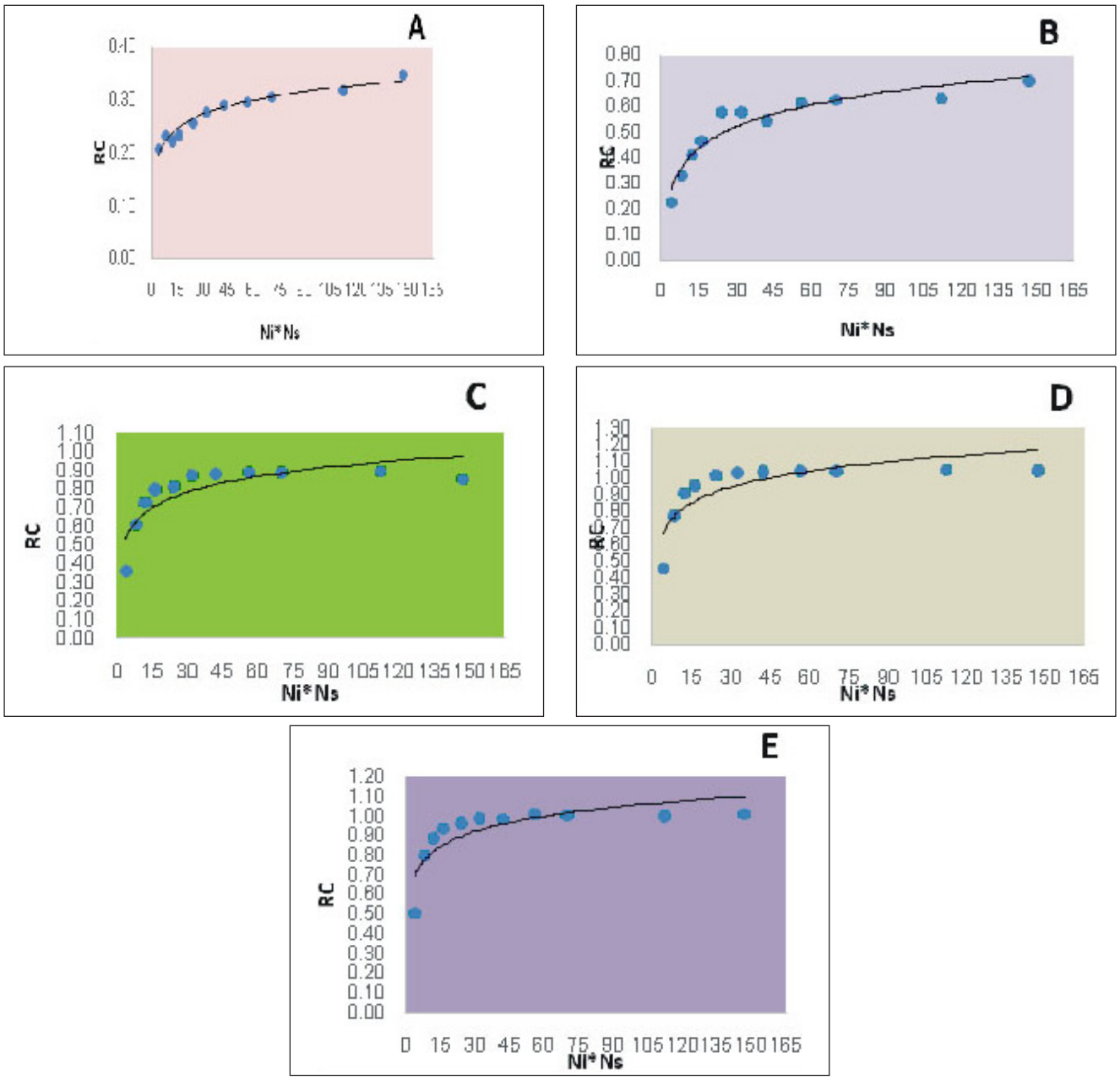

Fig. 1 : TrueX, TBR8, RC versus Ni*Ns shows that recovery coefficient for syringe 2.2cm is closer to the optimal value than the other syringes. A-Syringe 0.5cm, B- Syringe 0.9cm, C- Syringe 1.3cm, D- Syringe 1.6 cm, E- Syringe 2.

The background noise for each of the selected ROIs, σ_B^j was calculated based on the following formula.

$$\sigma_B^j = \sqrt{\frac{1}{N}\sum_{i=1}^{N}\left(A_{average} - A_i\right)^2} \quad (2)$$

Where, $A_{average}$ is the average activity inside each ROI, and A_i represents the activity of each voxel in the reconstructed image. The total background noise of the reconstructed image was measured based on the 20 defined ROIs in the background region of the aforementioned transverse slice as follows:

$$\sigma_B = \frac{1}{20}\sum_{j=1}^{20}\sigma_B^j \quad (3)$$

The limit of CNR as a detectability threshold is modified to be greater than 5 in this work. To find the best reconstruction parameters regarding detectability, the CNR parameter are measured for all 1380 configurations in the first day of imaging and the achieved results are compared for all the syringes.

Activity and recovery coefficient

The PET-reconstructed activity concentrations in each syringe for all the imaging time points are divided by the

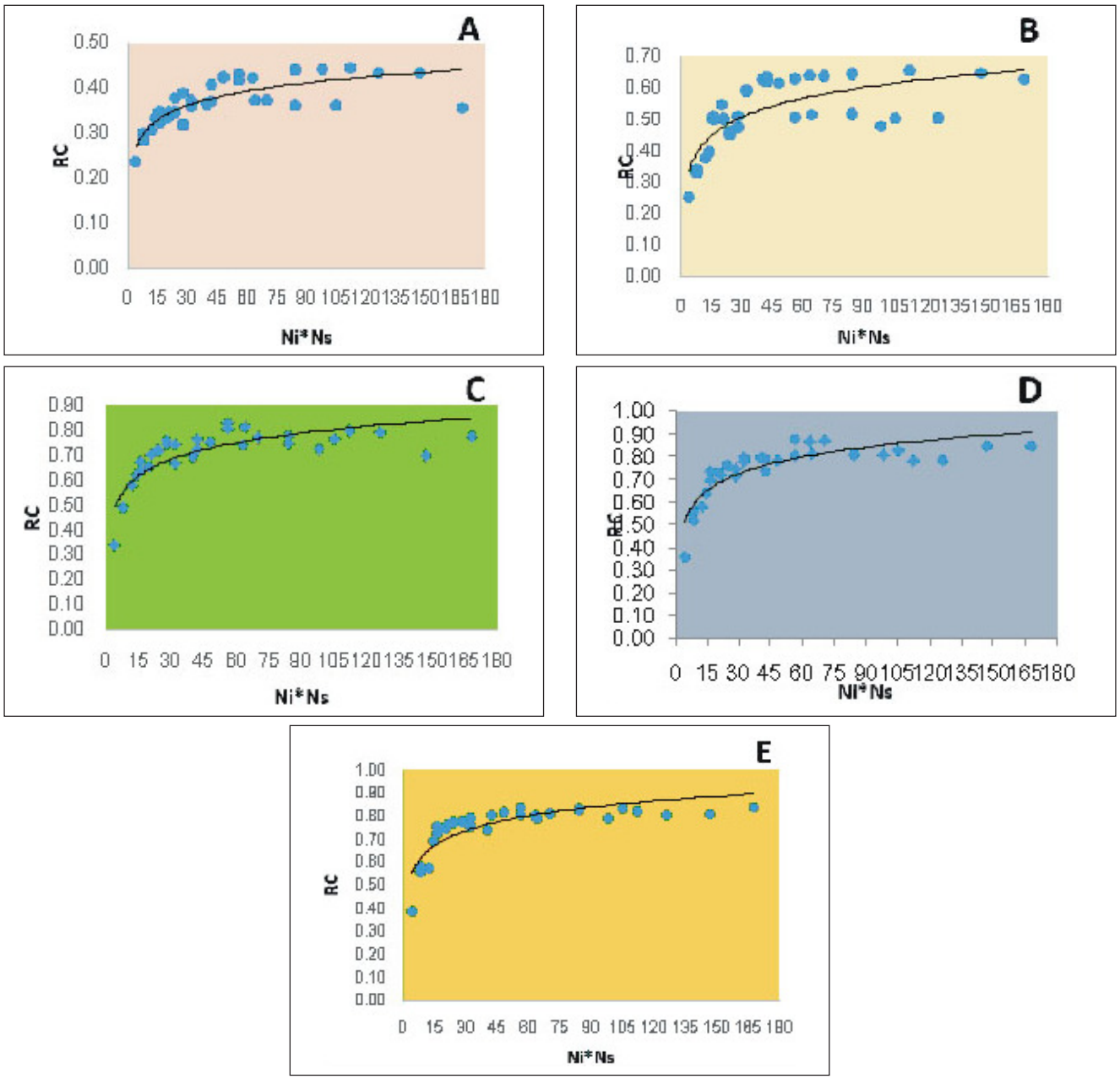

Fig. 2 : TrueX, TBR6, RC versus Ni*Ns shows that recovery coefficient for syringe 2.2cm is closer to the optimal value than the other syringes. A-Syringe 0.5cm, B- Syringe 0.9cm, C- Syringe 1.3cm, D- Syringe 1.6 cm, E- Syringe 2.2cm

calculated activity concentration as follows:

$$\text{Recovery coefficient} = \frac{Measured Concentration}{True Concentration} \times 100 \quad (4)$$

Recovery coefficient (RC) is plotted for syringes for all the syringes for all the different phantoms. The measured activity concentrations in each syringe are compared to the calculated values (True activity concentration) to evaluate the quantitative accuracy of the segmented VOIs. The difference between activity concentrations in the reconstructed VOIs and the true activity concentration is calculated.

Quantification accuracy and precision

In this study, the reconstructed PET and corresponding CT data at each imaging time-point were used to delineate five hot syringes in the phantom. The VOIs are defined based on a determined percentage of the maximum PET intensity. The percentage was chosen in such a way that we achieved the highest conformation between the volumes measured from CT and PET images. The mean intensity of all voxels inside this VOI defines the activity concentration in the corresponding volume

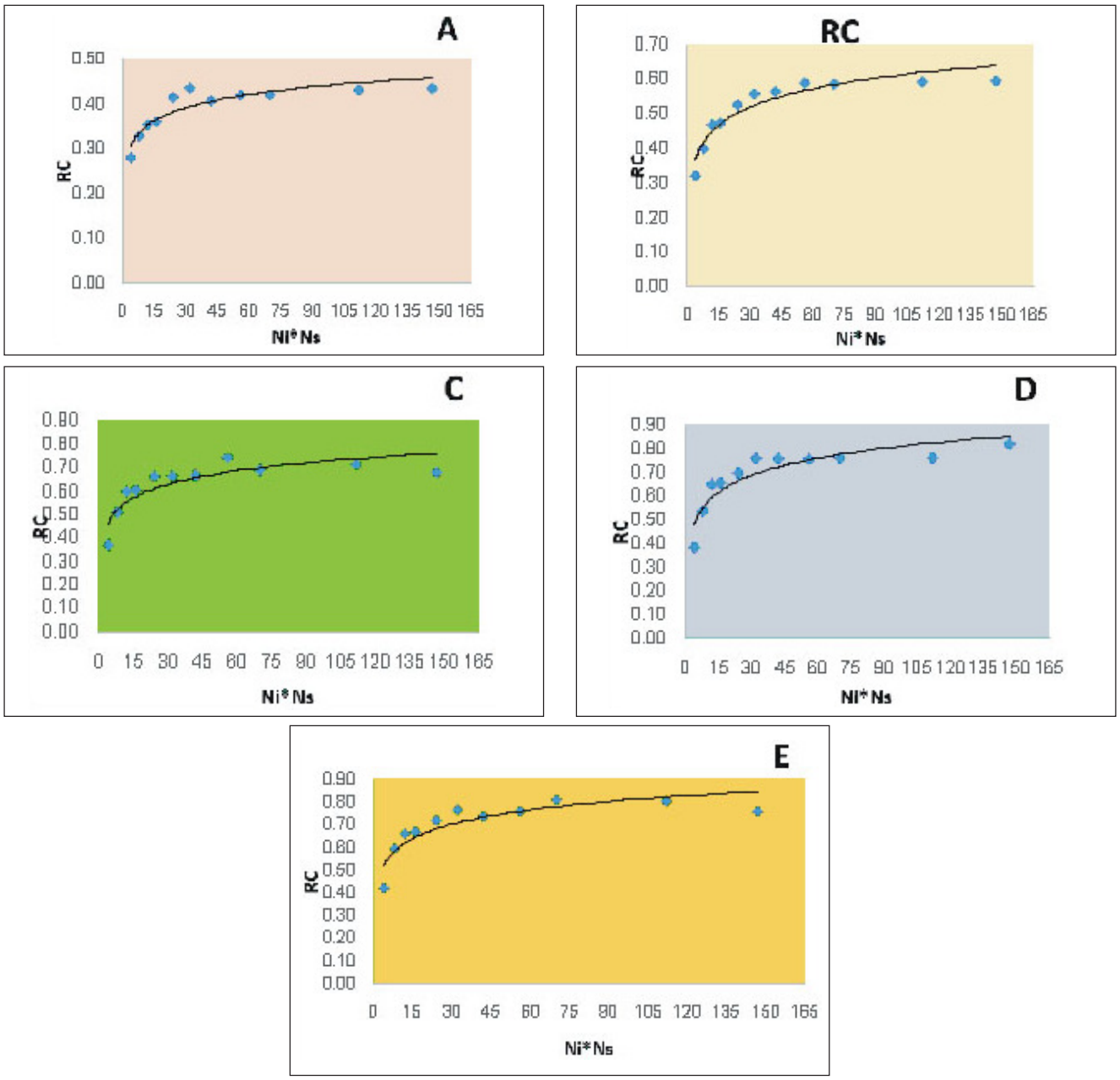

Fig. 3 : TrueX, TBR4, RC versus Ni*Ns shows that recovery coefficient for syringe 2.2cm is closer to the optimal value than the other syringes. A-Syringe 0.5cm, B- Syringe 0.9cm, C- Syringe 1.3cm, D- Syringe 1.6 cm, E- Syringe 2.2cm.

which is associated with the standard deviation (SD). The accuracy of this measured activity concentration is indicated as the percentage difference between the expected and measured values. To measure the precision of the obtained data, SD is indicated in terms of the mean activity concentration. This parameter which is also referred as the coefficient of variation (CoV) is calculated as follows:

$$\text{CoV}\ (\%) = \frac{SD}{Mean} \times 100 \qquad (5)$$

The accuracy and CoV of the reconstructed activity concentrations for four different phantoms are measured for all aforementioned reconstruction parameters.

RESULTS

RC for different TBRs, Syringe sizes and Reconstruction algorithms

To calculate the recovery coefficient for syringes activity concentrations, we divided the image value on the true value using equation (4). We plotted recovery coefficient in the hot syringes versus Ni*Ns (simply shown as Ni×Ns) for five different syringe sizes, 3 different

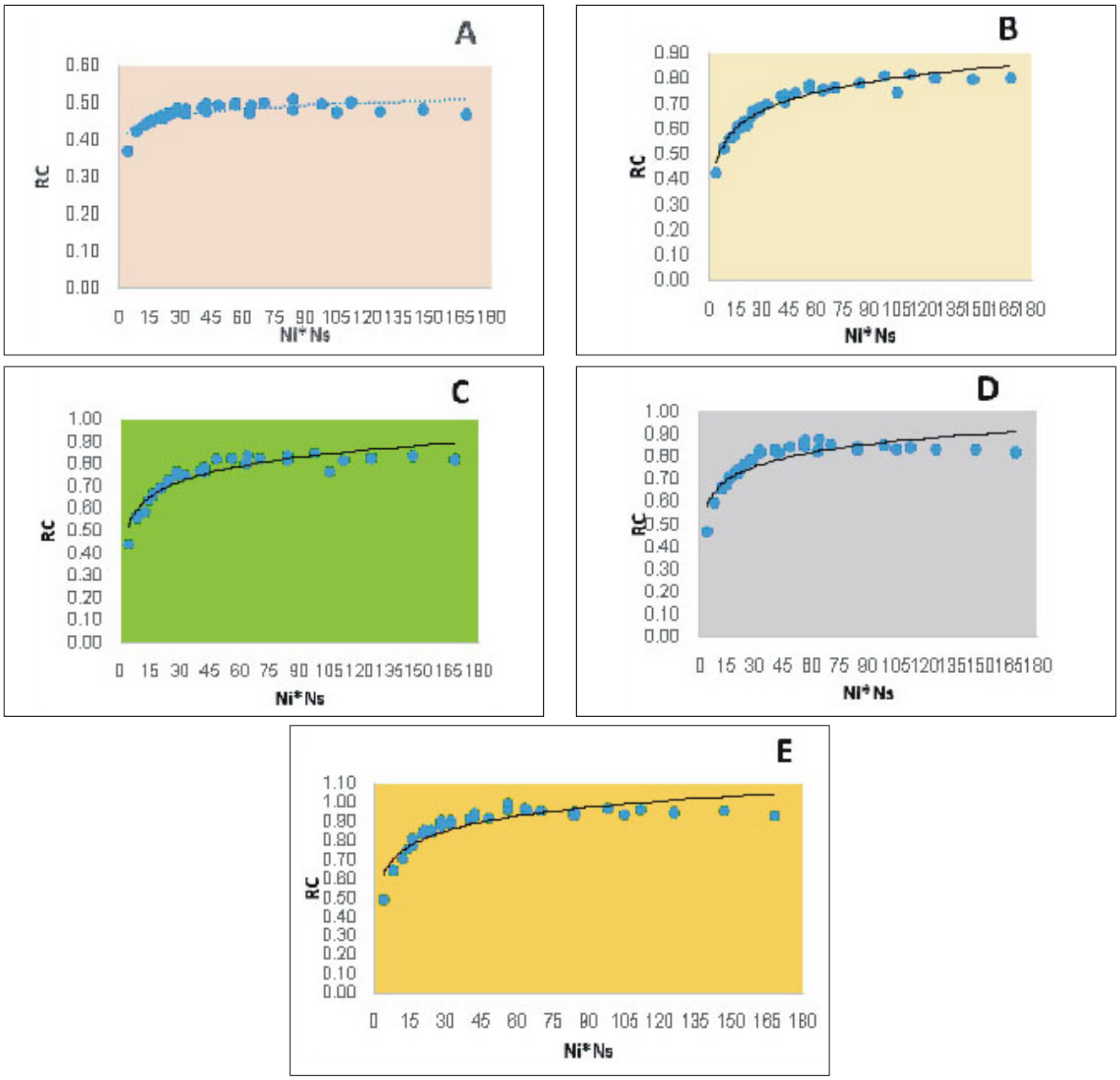

Fig. 4 : TrueX, TBR2, RC versus Ni*Ns shows that recovery coefficient for syringe 2.2cm is closer to the optimal value than the other syringes. A-Syringe 0.5cm, B- Syringe 0.9cm, C- Syringe 1.3cm, D- Syringe 1.6 cm, E- Syringe 2.

reconstruction algorithms and four TBRs. syringes.

The plots showed that the RC values for different syringe sizes of 0.5cm to 2.2 cm with TBR 8. The RC values reach near 1 for higher syringe sizes with TrueX algorithm (Fig. 1).

The same trend is seen for TBR 6 (Fig 2) and TBR 4 (Fig 3). For TBR2 (Fig. 4) the RC values improve for TrueX even in the lowest TBR value.

We noticed when the number of the sub-iterations increased, the estimated values for recovery coefficient are increased as well until their curve reaches a plateau. Further increasing the number of the iterations would not alter the value of the estimated activity concentration.

CNR and Detectability

In general, it is observed that changing the reconstruction parameters result in different CNR values based on size and TBR values. To calculate the CNR and detectability values for syringes we used equation (1). Our plots represent that CNR values for the hot syringes versus Ni*Ns for five different syringe sizes, different reconstruction algorithms and four TBRs. In this study, we aim to consider CNR values more than five. As CNR

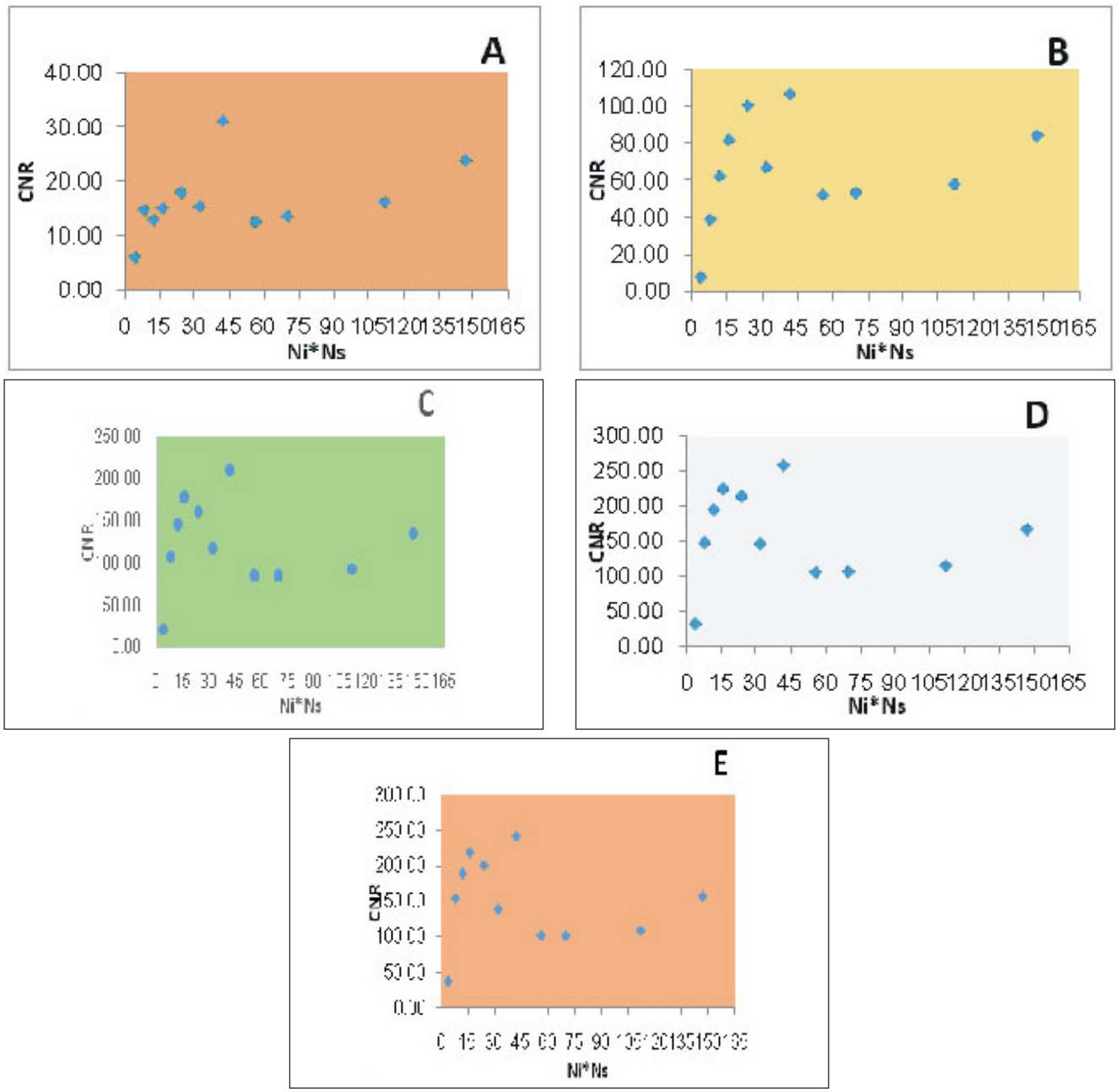

Fig. 5 : TrueX, TBR8, CNR versus Ni*Ns shows that contrast to noise ratio values for syringe 2.2cm is higher than the other syringes. A- Syringe 0.5cm, B- Syringe 0.9cm, C- Syringe 1.3cm, D- Syringe 1.6 cm, E- Syringe 2.2cm.

Table 1 : True values of phantoms activity concentrations.

TBR	8:1	6:1	4:1	2:1
Bkg. true value(MBq/cc)	0.0443	0.0447	0.0278	0.0457
Syringes true value (MBq/cc)	0.3544	0.2682	0.1112	0.0914

values are more than 50 for TBRs of 8 and 6 only a summarized results has been shown in this section. Plots showed that the CNR values for TBR 8 (Fig. 5) and TBR 6 (Fig. 6) for 5 different syringe sizes and 3 different reconstruction algorithms (iterative 2D, iterative 3D and TrueX).

It should be noted that TrueX behavior becomes worse (*i.e.* CNR becomes lower than 5) for smaller syringes and sub-iterations below 15. The CNR values decreases in TBR 4 for both 0.5 cm and 0.9 cm syringes in all reconstruction algorithms. TrueX behavior becomes worse even in the 1.3 cm syringe (Fig. 7).

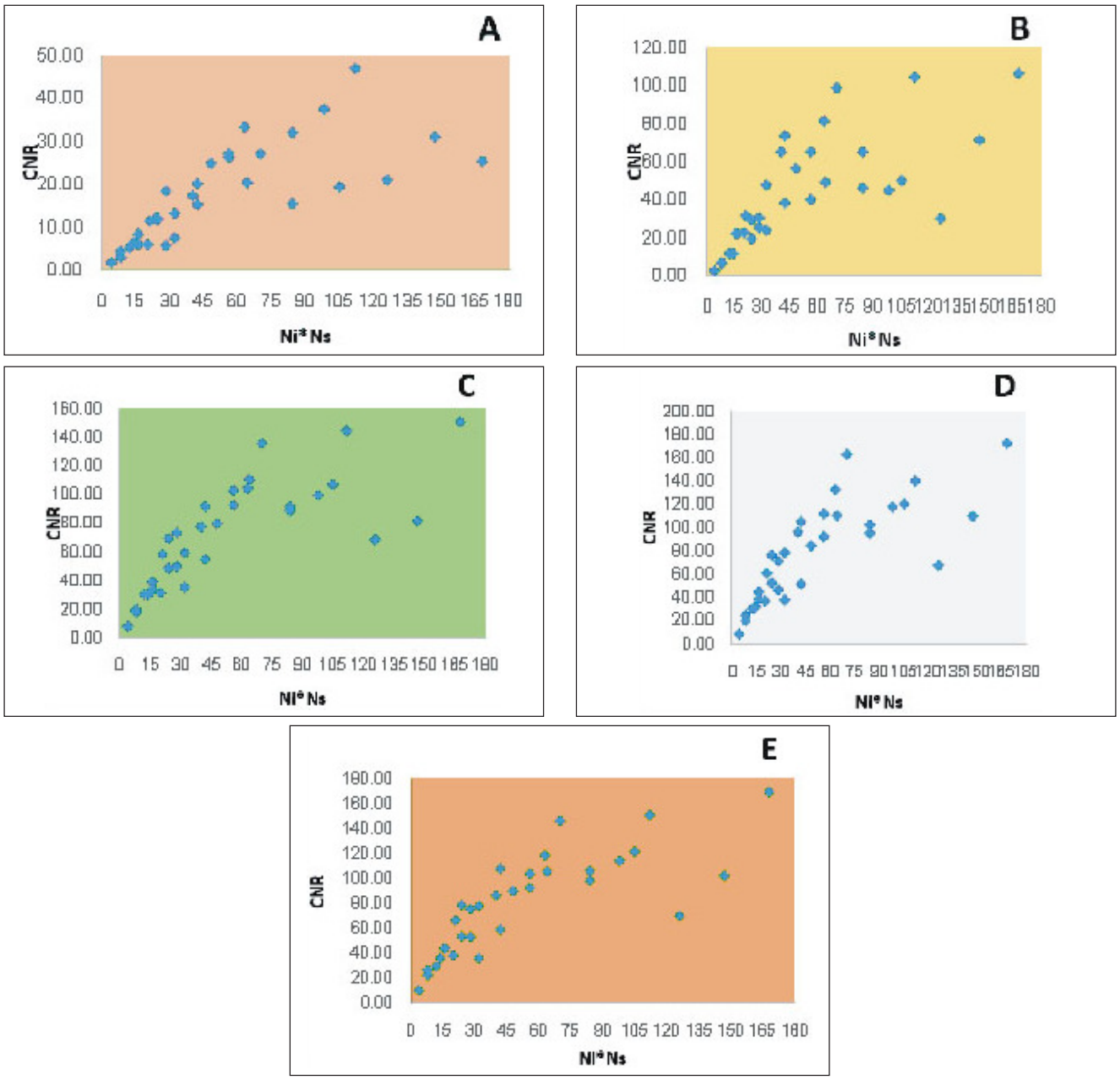

Fig. 6 : TrueX, TBR6, CNR versus Ni*Ns shows that contrast to noise ratio values for syringe 2.2cm is higher than the other syringes. A- Syringe 0.5cm, B- Syringe 0.9cm, C- Syringe 1.3cm, D- Syringe 1.6 cm, E- Syringe 2.2cm.

We noticed that negative CNR values for TBR2 and syringe 0.5 cm for all reconstruction algorithms which indicates no detectability (Fig. 8). And we noticed also when the number of the sub-iterations increased, the estimated values for CNR are not necessarily increased as well. It is mainly because CNR values were affected by more variation in higher iterations.

Quantitative accuracy and precision

For each set of the reconstruction parameters, the activity concentration (in MBq mL^{-1}) for various hot syringes were calculated based on the reconstructed PET/CT images. To find the optimized reconstruction parameters regarding quantitative accuracy, CoV and accuracy values for all activity concentrations and reconstruction parameters are considered.

In general, a smaller CoV (SD compared to the mean value) shows higher precision. In this work, reconstruction parameters which estimate activity concentration with high precisions and accuracy values are proposed. We plotted the relative error versus coefficient of variation for all reconstructed activity concentration (Figs. 9, 10, 11, 12). These plotsshowed that COV (image noise) increases with higher number of iterations. For bigger syringe sizes we have lower percentage relative error

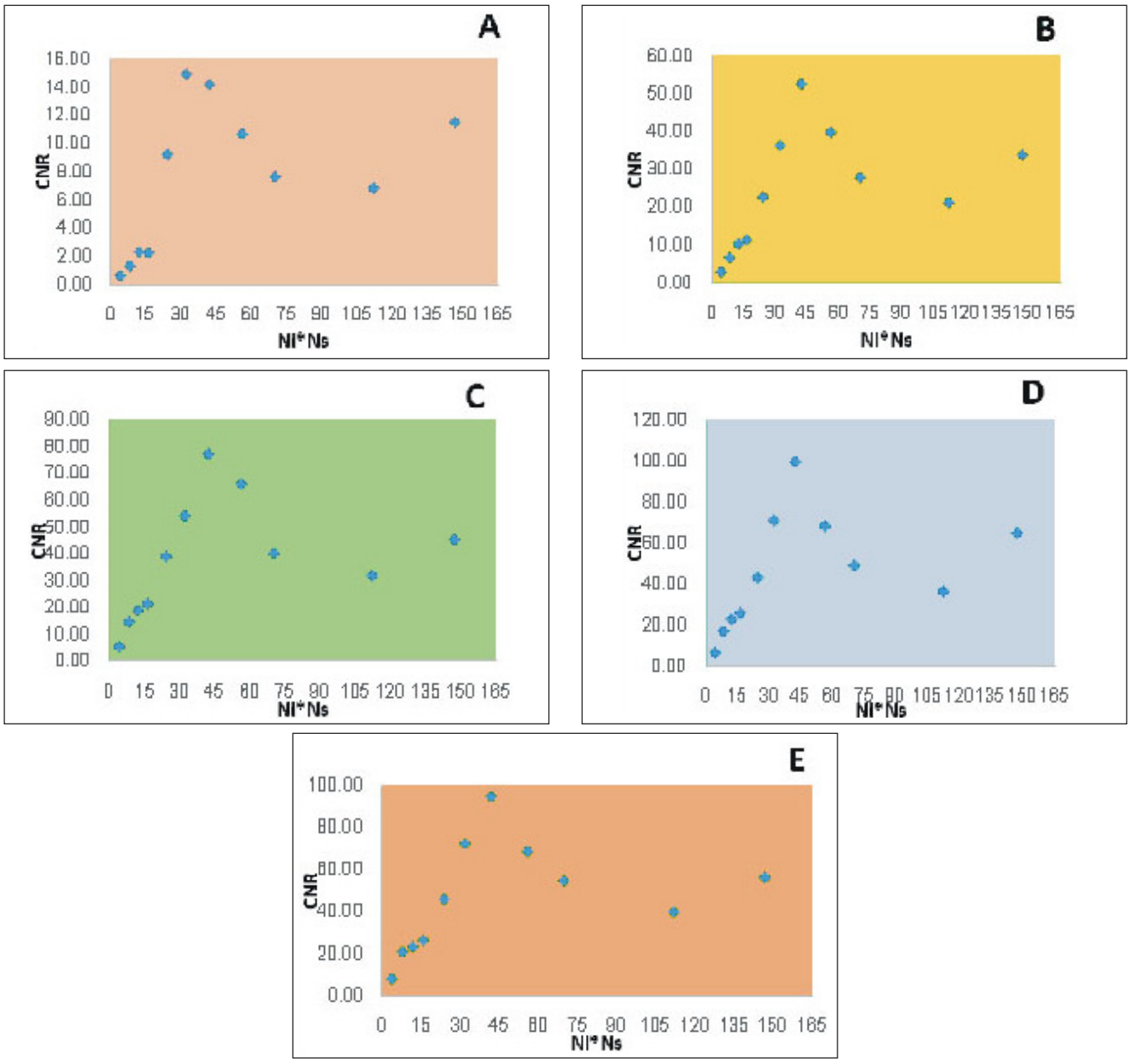

Fig. 7 : TrueX, TBR4, CNR versus Ni*Ns shows that contrast to noise ratio values for syringe 2.2cm is higher than the other syringes. A-Syringe 0.5cm, B- Syringe 0.9cm, C- Syringe 1.3cm, D- Syringe 1.6 cm, E- Syringe 2.2cm.

(higher accuracy) and lower COV (improved precision).

DISCUSSION

The aim of this study was to optimize the reconstruction parameters for a clinical PET/CT scanner in 18F-FDG imaging. The study was done using common reconstruction algorithms (2D, and 3D with and without resolution recovery). Image matrix size of 128 × 128, and post smoothing with 5-mm FWHM Gaussian filter.

Using a standard 128×128 image matrix size and 5-mm FWHM post-smoothing Gaussian filter, we examined several iteration and subset settings (sub-iterations showed as Ni×Ns) and evaluating contrast (CNR), recovery coefficient (RC), accuracy (as a function of percentage relative error) and precision (as a function of coefficient of variation- COV) for a range of tumor to background ratios (TBR) of 8, 6, 4 and 2 for different syringe sizes of 0.5 cm, 0.9 cm, 1.3 cm, 1.6 cm and 2.2 cm.

We noticed that RC values near one could define optimum sub-iterations for reconstructions. 2D iterative reconstructions could not be a good algorithm for small size lesions even in TBR values of 6 and 8. They show a bias even in 1.6 cm and 2.2 cm syringe sizes. We observed a similar trend in 3D iterative reconstruction for small lesion sizes even in TBR 8 for 1.6 syringe size. We

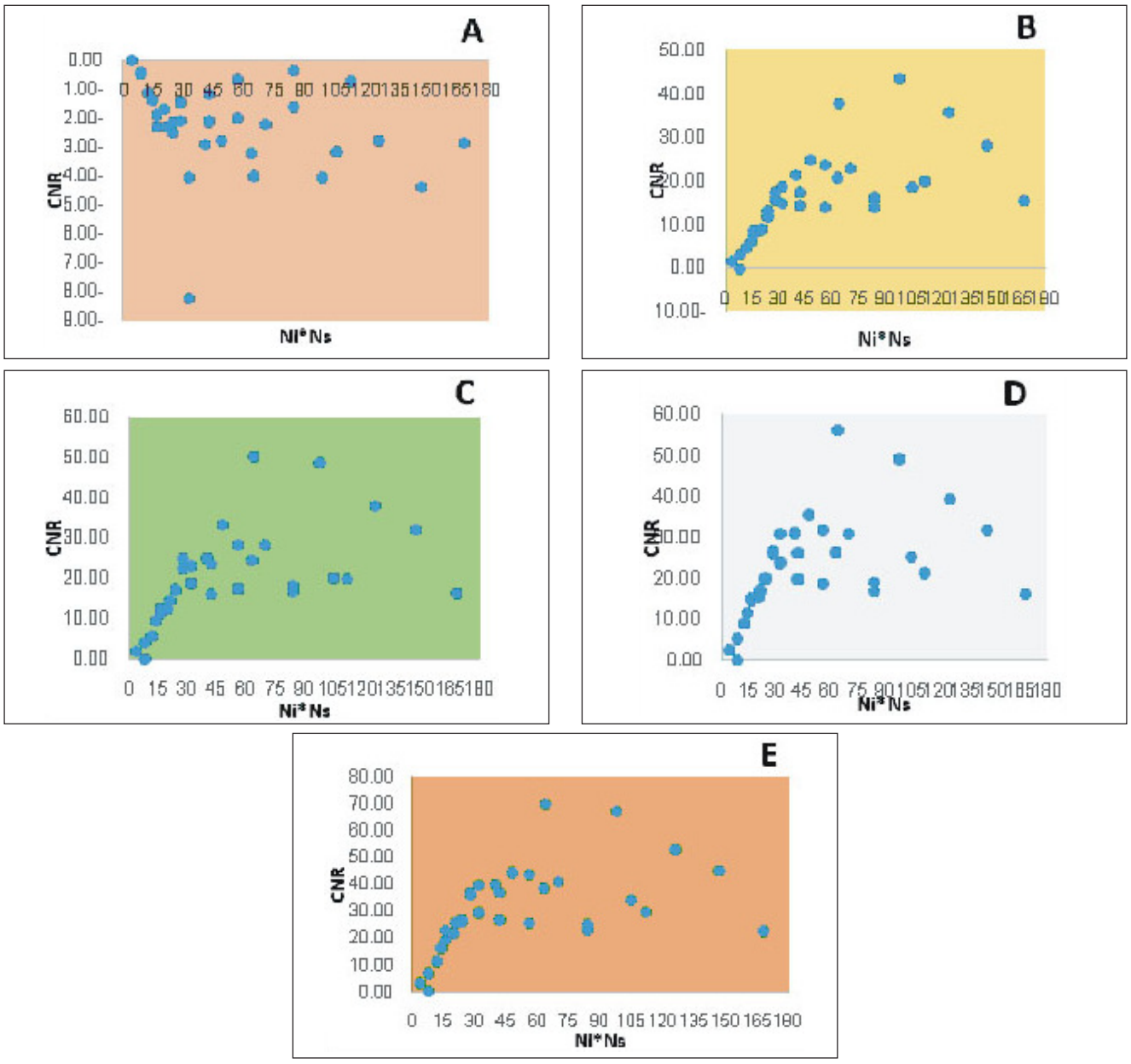

Fig. 8 : TrueX, TBR2, CNR versus Ni*Ns shows that contrast to noise ratio values for syringe 2.2cm is higher than the other syringes.In addition to that shows the negative CNR values for the smallest syringe and approach the low values for the others from zero. A-Syringe 0.5cm, B- Syringe 0.9cm, C- Syringe 1.3cm, D- Syringe 1.6 cm, E- Syringe 2.2cm.

concluded that it may be because of how we draw the ROI over the syringe. We used maximum conformity between PET and CT location of the syringe, for defining the region. The bias between the curve plateau and the true value may be reduced by drawing ROIs using a percentage threshold of maximum activity concentration.

Finally, TrueX is suggested in the reconstruction of small size syringes even in the low TBR levels. It is normally converges to the true quantification in sub-iterations approximately above 20. Thus, TrueX reconstruction with more than 20 sub-iterations is recommended.

Also we noticed that when the number of the sub-iterations increased, the estimated values for CNR are not necessarily increased as well. It is mainly because CNR values were affected by more variation in higher iterations. Therefore we investigate the influence of sub-iterations on the noise variation and related CNR values.

Using TrueX may result in CNRs below 5 for smaller syringes and sub-iterations below 15. Even in TBR 8, TrueX may result in CNRs below 5 in the 1.3 cm syringe size. It is mainly because low sub-iterations could not converge to the true image and further iterations are required for truly getting back the counts in to the image

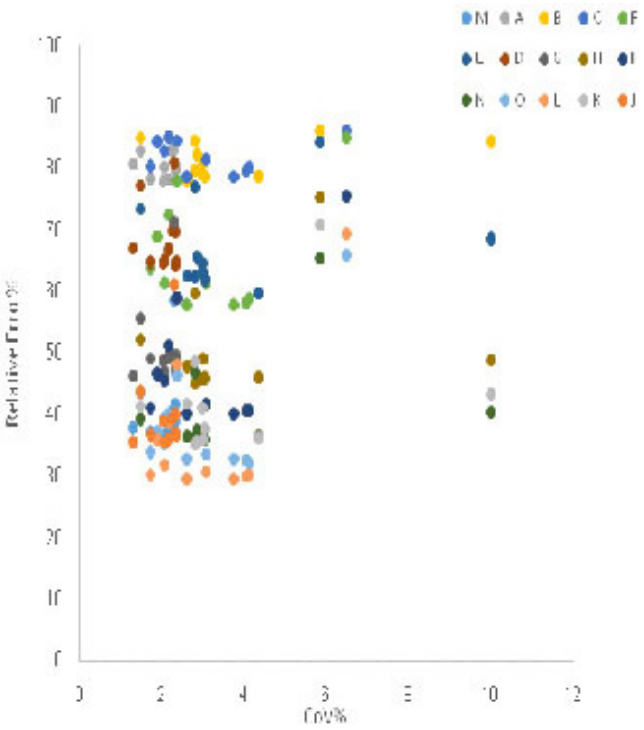

Fig. 9 : Percentage relative error versus coefficient of variation for all reconstructed activity concentration in TBR 8:1.
A- 2D syringe 0.5, B- 3D syringe 0.5, C- TrueX syringe 0.5, D- 2D syringe 0.9, E- 3Dsyringe 0.9,
F-TrueX syringe0.9, G-2D syringe1.3, H-3Dsyringe1.3, I-TrueX syringe1.3, J-2D syringe1.6,
K-3Dsyringe1.6, L- TrueX syringe1.6, M- 2D syringe2.2, N-3Dsyringe2.2, O-TrueX syringe2.2

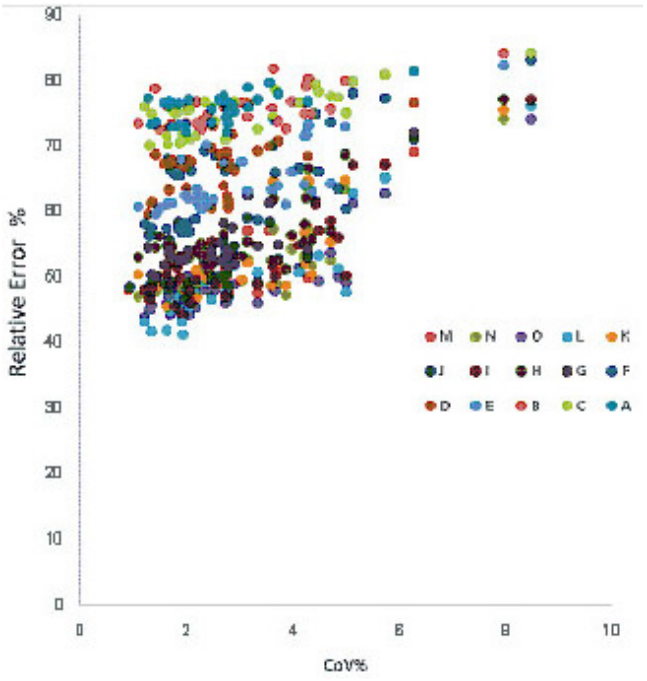

Fig. 10 : Percentage relative error versus coefficient of variation for all reconstructed activity concentration for TBR6:1
A- 2D syringe 0.5, B- 3D syringe 0.5, C- TrueX syringe 0.5, D- 2D syringe 0.9, E- 3Dsyringe 0.9,
F-TrueX syringe0.9, G-2D syringe1.3, H-3Dsyringe1.3, I-TrueX syringe1.3, J-2D syringe1.6,
K-3Dsyringe1.6, L- TrueX syringe1.6, M- 2D syringe2.2, N-3Dsyringe2.2, O-TrueX syringe2.2

objects. Thus we observed low CNR values in low sub-iterations even in TrueX reconstruction algorithm because additional information about the object needs to be recovered.

The CNR values decreases in TBR 4 for both 0.5 cm and 0.9 cm syringes in all reconstruction algorithms. We concluded that detecting small objects are more sensitive to sub-iteration number while more iterations are required for small size lesions accordingly.

It should be noted the CNR in phantoms with TBR8 and TBR 6 were superior to those with TBR4 and TBR2 as expected. Our results are consistent with previous studies reporting that the reconstruction algorithms were mainly responsible for the improvement in image quality. CNR and RC increased when the number of iterations increased (less than 60 sub-iterations).

Quantitative accuracy and precision are one of the most important issues in PET imaging. That is why we plot the accuracy versus precision to define which reconstruction algorithm can serve as the optimum for quantification purpose. To answer this, we plotted percentage relative error versus coefficient of variations to locate the optimum reconstruction algorithms in the region of lower relative error (higher accuracy) and lower COV (higher precision).

The percentage relative error versus COV for four TBR values. As shown in this study, lower COV (image noise) and lower percentage relative error (higher accuracy) belongs to L, O, N, F, I which are TrueX algorithm for both small and big sizes of syringes and K for 3D algorithm in a big size syringe. Nearly the same trend is observed for TBR levels of 6 and 4 respectively. However, behavior of reconstruction algorithms are very complicated in TBR 2 and small syringe sizes. It is mainly because small syringe sizes were not detectable in TBR2 and it makes a big challenge for the quantitative performance of aforementioned reconstruction algorithms.

CONCLUSION

Image quality and quantitative accuracy are strongly influenced by reconstruction parameters. This thesis was compatible with a protocol for standardization of optimization FDG whole body PET studies. In this thesis, we evaluated the effects of image reconstruction algorithms on PET/CT image quality and proposed

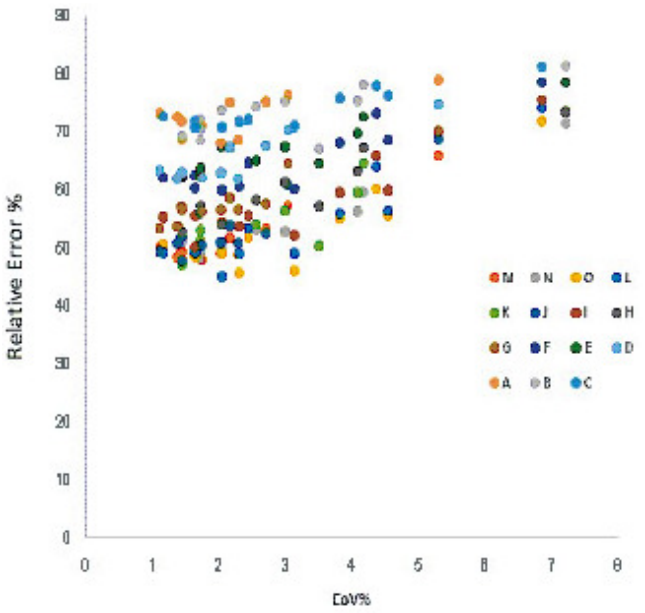

Fig. 11 : Percentage relative error versus coefficient of variation for all reconstructed activity concentration for TBR4:1.
A- 2D syringe 0.5, B- 3D syringe 0.5, C- TrueX syringe 0.5, D- 2D syringe 0.9, E- 3Dsyringe 0.9,
F-TrueX syringe0.9, G-2D syringe1.3, H-3Dsyringe1.3, I-TrueX syringe1.3, J-2D syringe1.6,
K-3Dsyringe1.6, L- TrueX syringe1.6, M- 2D syringe2.2, N-3Dsyringe2.2, O-TrueX syringe2.2

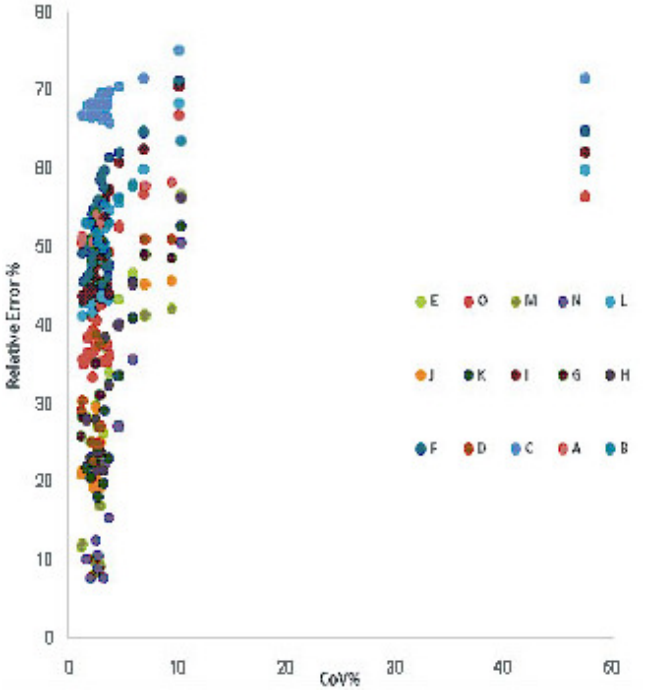

Fig. 12 : Percentage of relative error versus coefficient of variation for all reconstructed activity concentration for TBR2:1.
A- 2D syringe 0.5, B- 3D syringe 0.5, C- TrueX syringe 0.5, D- 2D syringe 0.9, E- 3Dsyringe 0.9,
F-TrueX syringe0.9, G-2D syringe1.3, H-3Dsyringe1.3, I-TrueX syringe1.3, J-2D syringe1.6,
K-3Dsyringe1.6, L- TrueX syringe1.6, M- 2D syringe2.2, N-3Dsyringe2.2, O-TrueX syringe2.2

reconstruction parameters which were distinctly optimized for quantification and detection of lesions. Higher sensitivity and improved image quality resulting from optimum image reconstruction parameters may be used to reduce the ^{18}F-FDG dose and shorten the scan duration. In this regard, TrueX image reconstruction with iterations more than 20 are proposed for different sizes of syringes and different TBR levels. It is worth noting that 5-mm FWHM post smoothing Gaussian filter and 128 by 128 image matrix size were considered in all reconstruction settings.

REFERENCES

Adams M C, Turkington T G, Wilson J M and Wong T Z (2010) A systematic review of the factors affecting accuracy of SUV measurements. *American Journal of Roentgenology* **195**(2), 310-20.

Anna Pees†a A J P, Romano V and Albert D. Windhorst. Fluorine-18 labelled building blocks for PET tracer synthesis. Department of Radiology & Nuclear Medicine, VU University Medical Center, Amsterdam, De Boelelaan 1085c, 1081 HV Amsterdam, The Netherlands.

Carlson S (1995) A glance at the history of nuclear medicine. *Acta oncologica* **34**(8), 1095-102.

Chen W and Dilsizian V (2015) PET assessment of vascular inflammation and atherosclerotic plaques: SUV or TBR? *Journal of Nuclear Medicine* **56**(4), 503-4.

Cherry S R S J and P M E (2003) *Physics in Nuclear Medicine*. Pennsylvania Elsevier. **3**rd edition ed.

Delbeke D, Coleman R E, Guiberteau M J, Brown M L, Royal H D, Siegel B A and Stabin M G (2006) Procedure guideline for tumor imaging with 18F-FDG PET/CT 1.0. *Journal of Nuclear Medicine* **47**(5), 885-95.

Faasse T and Shreve P (2008) Positron emission tomography–computed tomography patient management and workflow. In *Seminars in Ultrasound, CT and MRI WB Saunders*. August **29**(4), 277-82.

Makris N E, Huisman M C, Kinahan P E, Lammertsma A A and Boellaard R (2013) Evaluation of strategies towards harmonization of FDG PET/CT studies in multicentre trials: comparison of scanner validation phantoms and data analysis procedures. *European Journal of Nuclear Medicine and Molecular Imaging* **40**(10), 1507-15.

Medical Uses of Radioactive Materials. nuclear medicine radio chemistry society.

Moscariello A, Takx R A, Schoepf U J, Renker M, Zwerner P L, O'Brien T X and Fink C (2011) Coronary CT angiography: image quality, diagnostic accuracy, and potential for radiation dose reduction using a novel iterative image reconstruction technique—comparison with traditional filtered back projection. *European Radiology* **21**(10), 21-30.

Ng S C V H L, Law M W, Liu R K, Ma V W and Tso W K *et al* (2013) Patient dosimetry for 90Y selective internal radiation treatment based on 90Y PET imaging. *J. Appl. Clin. Med. Phys.* **14**, 212-21.

Ruth E, Schmitz A M A and Paul E Kinahan. The physics of PET/CT scanners. Imaging Research Laboratory Department of

Radiology University of Washington.

Teo B K, Seo Y, Bacharach S L, Carrasquillo J A, Libutti S K, Shukla H and Franc B L (2007) Partial-volume correction in PET: validation of an iterative post reconstruction method with phantom and patient data. *Journal of Nuclear Medicine* **48**(5), 802-10.

Tong S, Alessio A M and Kinahan P E (2010) Image reconstruction for PET/CT scanners: past achievements and future challenges. *Imaging in medicine* **2**(5), and 529.

What is nuclear medicine. Society of Nuclear Medicine.